IEEE Access
Multidisciplinary | Rapid Review | Open Access Journal

Received December 23, 2020, accepted January 9, 2021, date of publication January 22, 2021, date of current version February 4, 2021.

*Digital Object Identifier 10.1109/ACCESS.2021.3053626*

# Characterization and Model Parameters of Large Commercial Supercapacitor Cells

**ANTONIO MORANDI[1], (Senior Member, IEEE), ALESSANDRO LAMPASI[2], (Member, IEEE), ALESSANDRO COCCHI[3], FILIPPO GHERDOVICH[4], UMBERTO MELACCIO[1], PIER LUIGI RIBANI[1], (Member, IEEE), CLAUDIO ROSSI[1], AND FRANCESCA SOAVI[5]**

[1]Department of Electrical, Electronic, and Information Engineering, University of Bologna, 40136 Bologna, Italy
[2]National Agency for New Technologies, Energy, and Sustainable Economic Development (ENEA), 00044 Frascati, Italy
[3]Department of Astronautics, Energy, and Electrical Engineering, University of Rome Sapienza, 00184 Rome, Italy
[4]OCEM Power Electronics, 40056 Bologna, Italy
[5]Department of Chemistry "Giacomo Ciamician", University of Bologna, 40126 Bologna, Italy

Corresponding author: Antonio Morandi (antonio.morandi@unibo.it)

**ABSTRACT** The paper reports the results of the test and modelling activities carried out on large commercial supercapacitor cells at high current. Four commercials cells, with rated capacitance of 3000 F and rated voltage of 2.7 V, are considered. All cells are submitted to consecutive charge/discharge cycles at constant current. A test current in the range 80-130 A is used, which is comparable with the maximum operating current (up to 150 A) that the cells can reach in practical operations. A circuit model of the cells, able to reproduce the most relevant dynamic behavior, with a good compromise between accuracy, simplicity and robustness of the model's parameters, is also developed and validated against the experimental data. It is shown that all the investigated commercial cells are characterized by similar phenomena and comply with the same circuit model. Moreover, it is shown that the circuit parameters of the cells are in the same range and are weakly dependent on the test current. The obtained circuit parameters are accurately reported for all the cells and made fully accessible to users.

**INDEX TERMS** Supercapacitor, ultracapacitor, energy storage, supercapacitor test and modeling, equivalent circuit, supercapacitor efficiency, capacitance, high-current charge/discharge.

## I. INTRODUCTION

Supercapacitors (SCs) are electrochemical energy storage devices characterized by high power density and extremely high number of charge/discharge (CD) cycles without degradation [1], [2]. For these reasons, they found a wide range of applications in transportations, in industrial systems and in electric power grids. In particular, SCs are exceptionally effective when repetitive pulsed power is required [3], [4], [5]. Furthermore, the integration of SCs into hybrid solutions, like their combination with energy-intensive sources as lithium-ion batteries, appears as the potential key approach for future flexible and cost-effective energy storage devices or systems [1], [4], [6]–[9]. SC technology has nowadays reached a high level of maturity, with multiple products (cells and modules) that can be found on the market, spanning a wide range of ratings and provided by multiple manufacturers.

The associate editor coordinating the review of this manuscript and approving it for publication was Eklas Hossain.

Predicting the cells' behavior in different operating conditions is a main requirement of the proper exploitation of the SC potential. More in particular, experimental characterization of SC cells is required for evaluating their performance (and limits) under realistic operating conditions in view of practical applications and a reliable cell model, validated in realistic operating regimes, is also of utmost importance for the design and the optimization of the SC systems employing multiple cells. Intense research activities have been carried out so far concerning the characterization [2], [10]-[15] and the modelling [2], [16]–[32] of commercial SC cells available on the market. However, most of the characterization and modelling studies reported in the literature apply test currents that are very limited with respect to the practical operating currents of SC cells, that can reach up to 150 A. In particular, a large part of the studies reported in the literature are based on EIS approaches, with applied test currents typically $\ll$1 A). AC test at 1 kHz with small test current is considered in the IEC standard for the definition of the AC resistance of

the cell [15]. Cell characterization by means of CD cycles at constant current, which are more representative of the typical operation of SCs in applications, is also common, but the used test current is typically in the order of few amperes or tens of amperes at most.

In this paper the results of testing of SCs at high current values, reaching the maximum operating current of the cells, are presented. In particular, the performance of four commercial SC cells in the range 80-130 A are measured and compared by means of constant-current tests. The considered cells, having rated capacitance of 3000 F and rated voltage of 2.7 V, are among the ''largest standard'' products available on the market. Based on the characterization results the paper also develops an equivalent circuit model of the considered cells, able to reproduce the measured behavior in the whole tested current range. A phenomenological approach is followed for developing the model, whereby a compromise is looked for between the accuracy, its simplicity and the robustness of the parameters' identification procedure. The parameters of the equivalent circuit are identified by fitting of the measured data. The obtained parameters are accurately reported in the paper for all the cells and made fully available to users.

The paper is organised as follows: the main characteristics of the cells and the experimental setup are described in Section II. Section III compares for the commercial cells in terms of energy efficiency, coulombic efficiency and the differential capacity. In Section IV the equivalent circuit of the cells is introduced and the role of the different components of the circuit is highlighted. In Section V the parameters of the equivalent circuit of all cells and all operating currents are found by fitting the model generated data onto the experimental data. The comparison between numerical and measured results is shown and discussed. Concluding remarks are drawn in Section VI.

## II. EXPERIMENTAL SET-UP AND PROCEDURE

### A. COMMERCIAL SC CELLS

The experimental activities were focused on SC cells with the ''largest standard'' size, namely having the maximum value of capacitance/energy. Four commercially available SC cells were identified [33]–[36]. The main characteristics of the cells, as declared by the manufactures, are summarized in Table 1. Though produced by four different and independent manufactures, the cells have very similar characteristics that are representative of the SC technology. In particular:

- All cells have cylindrical shape (which is the most common layout for SCs cells), with identical diameter (60.7 mm) and length (138 mm).
- The rated voltage $V_r$ (that is, the maximum operating voltage in normal condition) is identical for all the cells (2.7 V). In practice, this is a standard for present SC technology (though different $V_r$ values, up to 2.85÷3 V, exist now on the market [37], [38]).
- The rated capacitance $V_r$ is identical for all the cells (3000 F). Cells with smaller capacitance are widely available on the market but are less interesting for energy storage applications and not used for integrated modules. On the other hand, few examples of cells with higher capacitances exist. It is important to stress that the rated capacitance reported is the minimal value assured and is normally exceeded in the practice, even by above 10% [3].
- The rated current $I_r$ (that is, the maximum the maximum continuous current producing an increase of temperature within 15 °C) is very similar and is in the range 128÷150 A).
- The equivalent series resistance (ESR) [15] is very similar for all cells and is in the range 0.23÷0.29 mΩ. Note that different definitions and measurement methods could have been adopted by the different manufactures for obtaining this parameter.
- The declared self-discharge rate (at 25 °C), related to the leakage resistance, is identical for all the cells.
- All cells have screwed terminals (external threads) for the connection to the test circuit.

**TABLE 1. Main characteristics of the four SC cells used in the experimental tests (in alphabetic order).**

| Manufacturer | EATON | LSUC | MAXWELL | SPSCAP |
|---|---|---|---|---|
| Product name | XL60 | EA ST01 | BCAP | 2R7STA |
| Rated voltage ($V_r$) | 2.7 V | 2.7 V | 2.7 V | 2.7 V |
| Rated capacitance ($C_r$) | 3000 F | 3000 F | 3000 F | 3000 F |
| Storable energy | 10.94 kJ 3.04 Wh | 10.94 kJ 3.04 Wh | 10.94 kJ 3.04 Wh | 10.94 kJ 3.04 Wh |
| ESR ($R_{ESR}$) | 0.23 mΩ | 0.23 mΩ | 0.29 mΩ | 0.29 mΩ |
| Rated continuous current ($I_r$) for $\Delta T$=15 °C | 143 A | 150 A | 130 A | 128 A |
| Self-discharge rate | <5%/ month | <5%/ month | <5%/ month | <5%/ month |
| Overall diameter | 60.7 mm | 60.7 mm | 60.7 mm | 60.7 mm |
| Overall length | 138 mm | 138 mm | 138 mm | 138 mm |
| Terminals | Screwed | Screwed | Screwed | Screwed |
| Source | [33] | [34] | [35] | [36] |

### B. TEST EQUIPMENT

The cells were charged and discharged at a controlled current by means of the circuit sketched in Figure 1. A one-quadrant power source (TDK Lambda GEN8) with 400 A / 8 V capability was used to supply the current to the test circuit. As the DC source can generate DC current only in one direction, a H-bridge made of power mosfet components was introduced in the circuit to invert the polarity of the test current [39] with high dynamic. Since the voltage of the power supply cannot be reversed, a dump resistor was added in series to the SC to keep an overall positive voltage over the source also during the discharge. The whole system was managed by means of a LabVIEW interface.

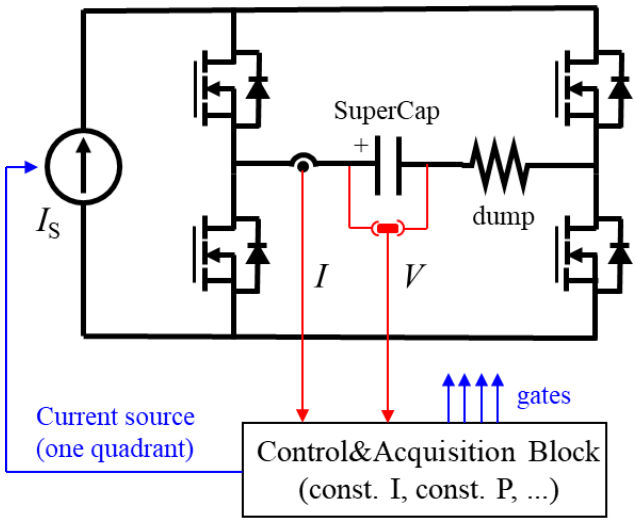


**FIGURE 1.** Schematic of the experimental set-up used for the test of the SC cells.

The Control and Acquisition Block in Figure 1 performs the following functions:

- Regulating the constant current $I_S$ of the current-source power supply.
- Commanding the four switches to reverse or interrupt the current flowing in the SC cell according to the desired operating mode and CD cycle.
- Continuously acquiring the SC voltage and current.

CD cycles at constant power, where the current $I_S$ of the power supply is regulated according to the actual voltage V of the cell (so that the product $V{\cdot}I_S$ is constant) can also be implemented by means of the system of Figure 1, but this function is not used in the paper.

### C. TEST PROCEDURE

The tests at constant current with high current value are relevant for applications of SCs in energy storage. The manufacturers normally suggest to limit the operating cycle of the cells to span a voltage range between the rated voltage $V_r$ and the 50% of this value, corresponding to a usable energy of 75% of the maximum storable energy [5], [9]. This voltage range was used in the tests.

Each SC cell was subjected to the following test procedure, exemplified in Figure 2 for the Maxwell cell with test current of 120 A:

1. Before starting the measurements, the cell was slowly pre-charged at the half of the maximum voltage (1.35 V). A current of 10 A was used during this phase.
2. The source current $I_S$ was set to the desired constant test value in the range 80÷130 A.
3. The cell was charged at constant current up its rated voltage (2.7 V).
4. A resting time of 10 s with no current supplied to the cell was waited before the following discharging phase.
5. The cell was discharged at constant current down to the half of the rated voltage (1.35 V), that is the typical limit for practical applications.
6. A resting time of 20 s with no current supplied to the cell was waited before the following cycle.
7. Four consecutive CD cycles were repeated with the same $I_S$.
8. The four test cycles were repeated for all the 6 values of $I_S$ in the range 80÷130 A with steps of 10 A.

The voltage during the two transient phases (at the end of discharge of the second cycle and at the end of the charge of the third cycle) is zoomed in Figure 2. A step change $\Delta V$ of the cell voltage can be observed at the end or begin of each CD phase, followed by a gradual time change during the waiting interval in which no current is supplied to the cell. The step change $\Delta V$ of the voltage is related to the step change $\Delta I$ of the current. This effect is exploited for obtaining the ESR (see Table 1), based on the assumption of an equivalent series RC circuit and according to the measurement method and extrapolation procedure specified in standard IEC 62391-1 [15].

## III. DEFINITION OF THE INDICATORS AND ANALYSIS OF THE PERFORMANCES OF THE SC CELLS

The analysis and the comparison of the cells' performance is carried out in the following based on different quantitative indicators.

### A. ENERGY LOSSES

The energy $E(t)$ absorbed by the cell from the begin of the tests can be calculated by integrating the instant absorbed power $P(t)$ of the cell, that is

$$E(t) = \int_0^t P(t')\,dt' = \int_0^t V(t') \cdot I(t')\,dt'. \tag{1}$$

Figure 3 shows the energy absorbed by the Maxwell cell during the CD cycles at ±120 A shown in Figure 2. A similar behavior was observed for all the cells in the whole range of currents.

In a cycle, the energy can be divided in the energy absorbed (because of the direction of the current) by the cell during the charge phase

$$E_c \stackrel{def}{=} \int_{t_{start}}^{t_m} V(t') \cdot I(t')\,dt' \tag{2}$$

and the energy returned (because of the reversed direction of the current) by the cell during the discharge phase

$$E_d \stackrel{def}{=} \int_{t_m}^{t_{end}} V(t') \cdot |I(t')|\,dt' \tag{3}$$

where $t_{start}$ and $t_{end}$ are the start and the end instant of the cycle respectively and $t_m$ is the middle point of the resting interval between charge and discharge. In case of ideal cells with no internal dissipation, as cyclic voltage operation is considered, the whole energy absorbed by the cell during the charge should be supplied back by the cell during the discharge, and no net energy

$$\Delta E = E_c - E_d \tag{4}$$

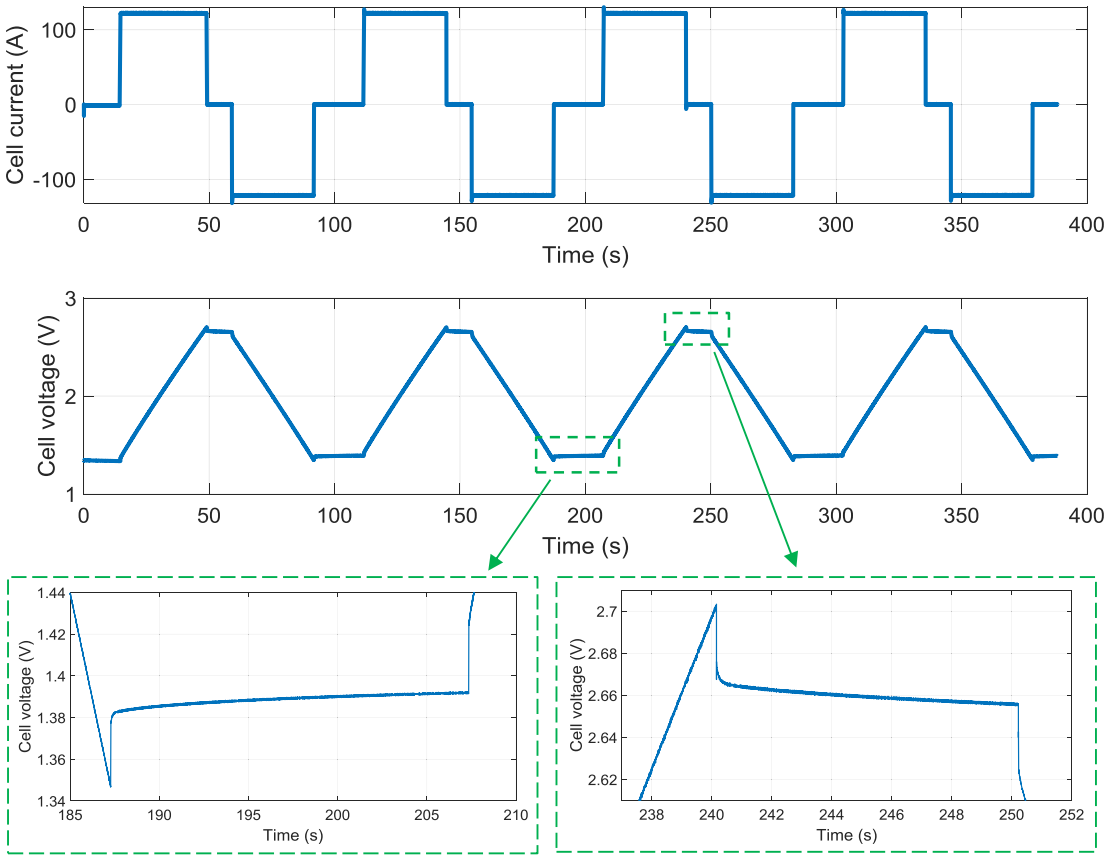


**FIGURE 2.** Waveforms of the cell current and voltage during the adopted test procedure with four CD cycles. The two inserts show the zoom of the transient phases at the end of each CD phase. The plotted waveforms refer to the Maxell cell with the test current set to $I_S = 120$ A.

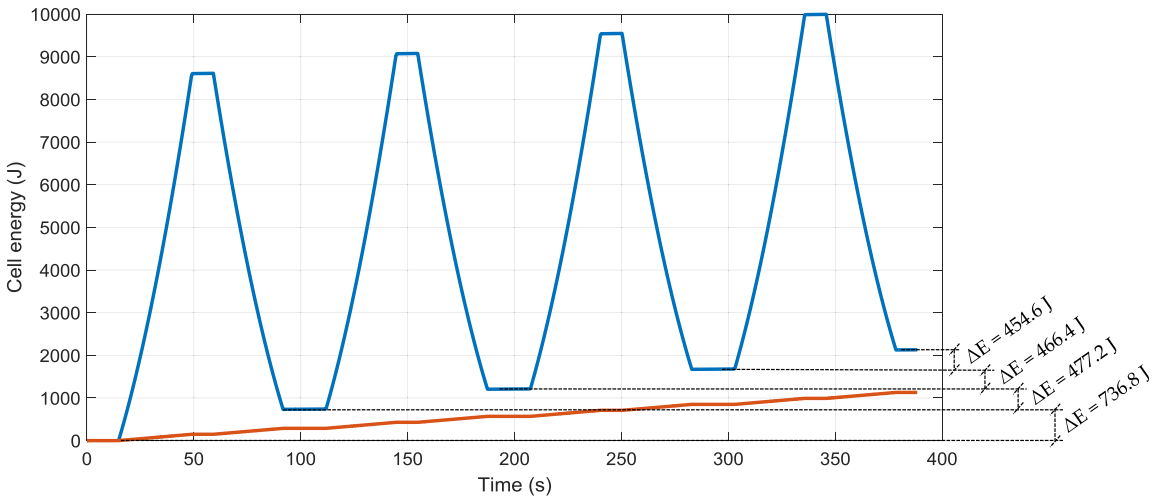


**FIGURE 3.** Evolution of the energy absorbed by the Maxwell cell during four CD cycles at ±120 A. The energy is absorbed by the cell during each charge phase (increasing energy) and is supplied back during each discharge phase (decreasing energy). The net energy $\Delta E$ of a cycle is not zero due to the internal dissipation. The dotted red line denotes the theoretical loss estimation obtained due to the ESR provided by the manufacturer.

should be absorbed in one cycle. In other terms, the value obtained from (4) should be zero at the end of each cycle. On the contrary, Figure 3 clearly shows that the net energy of one cycle is not zero, meaning that an internal dissipation occurs in the cell.

### *B. LOSS BEHAVIOR OF REPORTED EQUIVALENT RESISTANCE*

The cell dissipation is generally taken into account by means of a single equivalent series resistance $R_{\mathrm{ESR}}$ (see Table 1). In particular, the assumption of an equivalent series RC circuit,

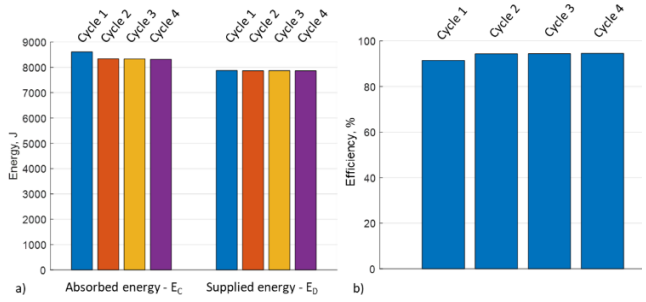


**FIGURE 4.** Absorbed/supplied energy and efficiency of the Maxwell cell during the four cycles with ±120A.

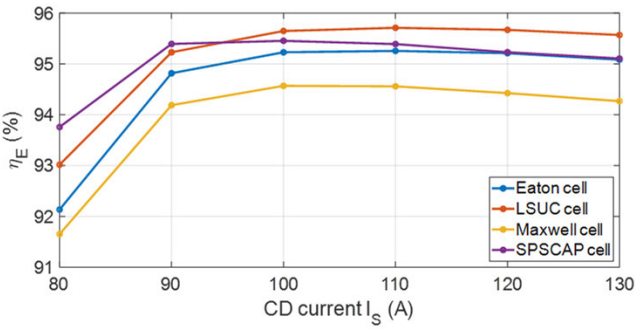


**FIGURE 5.** Energy efficiency of the four commercial SC cells during the CD cycles with constant current in the range 80÷130 A. Each efficiency was estimated as the average value of the cycles 2, 3 and 4.

with $R_{\mathrm{ESR}}$ in series with the capacitance, allows a simple estimation of the energy $E_{\mathrm{ESR}}(t)$ dissipated by the cell via the time integral of the instantaneous power loss, that is

$$E_{\mathrm{ESR}}(t) = R_{\mathrm{ESR}} \int_0^t I^2(t')\, dt' \tag{5}$$

The loss estimation obtained via (5) by using the nominal value of $R_{\mathrm{ESR}} = 0.29$ mΩ is also reported by the dotted red line in Figure 3. If the model underlying equation (5) was strictly valid, the calculated $E_{\mathrm{ESR}}(t)$ line should coincide, during the resting intervals between the discharge and charge phase, with the actual energy $E(t)$ absorbed by the cell, obtained by means of (1) from the measured current and voltage. The evident difference in the results means that the value of the ESR and/or the assumed equivalent series RC circuit need to be revised in order not to underestimate the observed loss behavior.

### C. ENERGY EFFICIENCY

The loss behavior can also be investigated in terms of energy efficiency $\eta_E$, that can be defined as the ratio between the energy $E_{\mathrm{d}}$ delivered by the cell during the discharge and the energy $E_{\mathrm{c}}$ absorbed during the charge [2], [13], that is

$$\eta_E \stackrel{def}{=} \frac{E_{\mathrm{d}}}{E_{\mathrm{c}}} = \frac{\int_{t_{\mathrm{m}}}^{t_{\mathrm{end}}} V(t') \cdot \left|I(t')\right| dt'}{\int_{t_{\mathrm{start}}}^{t_{\mathrm{m}}} V(t') \cdot I(t')\, dt'} \tag{6}$$

where $t_{\mathrm{start}}$, $t_{\mathrm{end}}$ and $t_{\mathrm{m}}$ have the same definition as for equations (2) and (3). The efficiency obtained for each cycle for the Maxwell cell during the CD cycles at ±120 A is shown in Figure 4, along with the energy absorbed and supplied in each cycle. It can be seen that a higher energy is absorbed in the first cycle. After that, the absorbed energy only slightly changes (<0.1%). The supplied energy is practically constant for all cycles. As a consequence, a lower efficiency of ≈91.4 % is obtained for the first cycle, whereas a practically constant efficiency of ≈94.4% is obtained starting from the second one.

It is worth to point out that the different energy behavior of the cell in the first cycle is inherent since, due to the effect of the resistive voltage drop, the voltage of the cell during the CD process with constant current becomes cyclic only after the first charge to the rated voltage $V_{\mathrm{r}}$. In other words, a larger energy is absorbed in the first cycle to compensate the lower initial voltage, but this does not correspond to a larger dissipation because part of this energy is kept in the capacitor at the end of the discharge (as the final voltage is higher than the initial one). As a consequence, the definition of efficiency given by (6) should only be used starting from the second cycle to characterize the loss behavior of the cell.

The measured energy efficiency $\eta_E$ of all the four considered cells, obtained by applying the CD-cycles at constant current in the range 80÷130 A is shown in Figure 5. For each cell and testing current, the average of the efficiency values $\eta_E$ measured during the second, third and fourth cycles are reported. As it can be observed in the figure, a quite flat efficiency behavior, in the range 94.3÷95.7%, is observed for a CD current in the range 100÷130 A, but two relevant phenomena must be pointed out:

1. The efficiency shows a slight decrease at higher operating current.
2. The efficiency shows a significant decrease at lower current, with a sudden drop (of about 2%) at the lowest operating current of 80 A.

All the analysed cells followed a similar behavior.

### D. COULOMBIC EFFICIENCY

For each cycle, the coulombic efficiency can be defined as the ratio between the charge $Q_{\mathrm{d}}$ delivered by the cell during the discharge phase and the charge $Q_{\mathrm{c}}$ that was injected during the charge phase [2], [13]:

$$\eta_Q \stackrel{def}{=} \frac{Q_{\mathrm{d}}}{Q_{\mathrm{c}}} = \frac{\int_{t_{\mathrm{m}}}^{t_{\mathrm{end}}} \left|I(t')\right| dt'}{\int_{t_{\mathrm{start}}}^{t_{\mathrm{m}}} I(t')\, dt'} \tag{7}$$

The measured coulombic efficiency of all cells during cyclic CD at constant current in the range 80 A - 130 A is shown in Figure 6. For all cells, a decrease of the coulombetric efficiency can be observed with the decreasing of the current, with a drop in the range 2-4% for the lowest operating current of 80 A.

### E. DIFFERENTIAL CAPACITANCE

The most evident behavior of a SC cell during constant-current operation is the gradual increase of the voltage with time, as it can be seen in Figure 2. Hence, as a very first

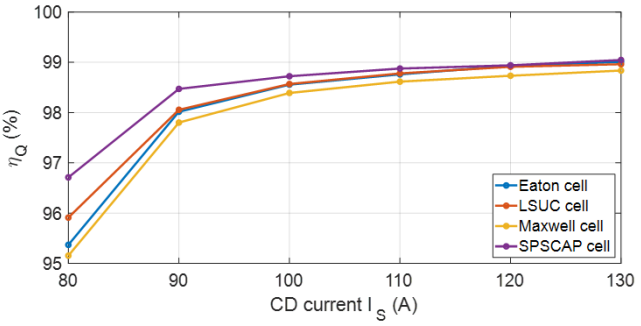


**FIGURE 6.** Coulombic efficiency of the four commercial SC cells during the CD cycles with constant current in the rage 80÷130 A. Each efficiency was estimated as the average value of the cycles 2, 3 and 4.

approximation, a simple capacitance can be assumed to model the cell. However, as discussed in Section IV, more elements need to be added in the equivalent circuit for accurately reproducing the overall behavior of the cell, that also includes the nonlinear voltage increase, the internal losses and the transient phases visible in Figure 2. Nevertheless, the simple capacitance model is widely used for gaining a first indication of the cell performance and for comparison purposes.

Different definitions and measurement techniques of the capacitance are possible, including differential, linear and integral capacitance [18], [10], [23]. The differential capacitance, obtained from the ratio between the current and the numerical derivative of the cell voltage [2], [14], [24] is discussed here:

$$C_{\text{diff}} \stackrel{def}{=} \frac{I}{dV/dt} \tag{8}$$

Figure 7 shows as an example the differential capacitance $C_{\text{diff}}$ of the Maxwell cell during the CD test at ±120 A. Even if the curves are affected by the typical noise of numerical derivative obtained from measured data, a linear increase of the differential capacitance with the cell voltage can be clearly observed, as widely reported in the literature [2], [14], [24] . The measured capacitance is in the range 2900-3400 F, which is consistent with the nominal capacitance of 3000 F (see Table 1), obtained by the manufacturers according to Standard IEC 62391-1 [15]. A discussion concerning the relationship between the differential and the nominal capacitance reported for commercial cells can be found in [18].

As shown in Figure 8, the capacitance $C_{\text{diff}}$ does not present a significant change in the four cycles, neither in charge nor in discharge. Moreover, a similar dependence $C_{\text{diff}}(V)$ on the voltage as those shown in Figure 7 was observed at different test currents and for all the commercial cells. An aspect to be noted is the dependence of $C_{\text{diff}}$ on the current direction (charge or discharge phase). A much flatter dependence was obtained during the discharge, with an average slope of 432 F/V. A much higher average slope of 660 F/V is instead obtained during the charge. This effect is also reported in [2] and [25].

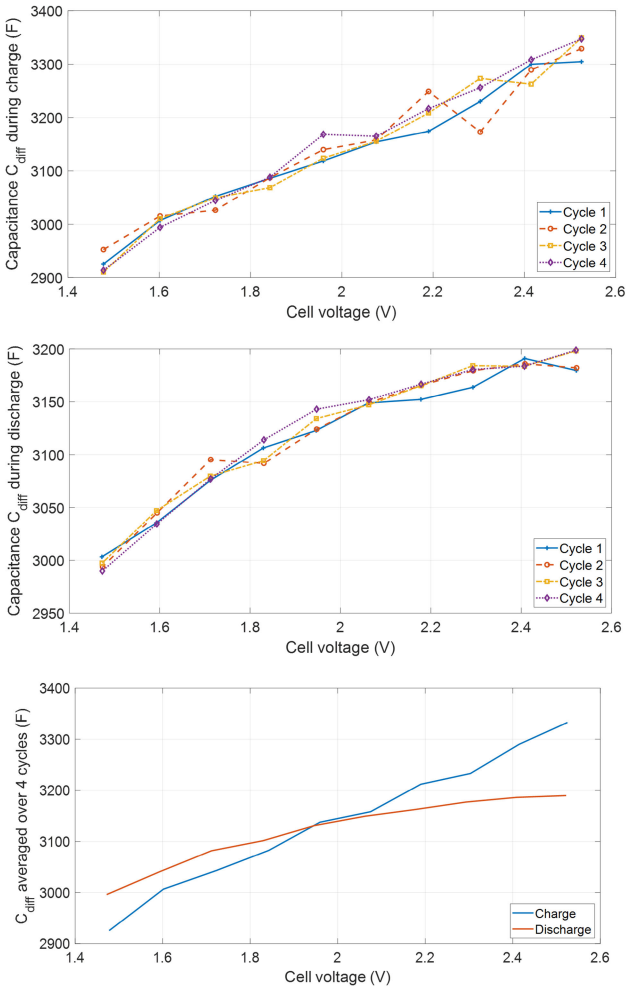


**FIGURE 7.** Differential capacitance $C_{\text{diff}}(V)$ of the Maxwell cell estimated during each charge (top plot) and discharge (middle plot) phase of the four cycles at ±120 A. The bottom plot compares the charge and discharge profiles obtained by averaging the measurements during the four cycles.

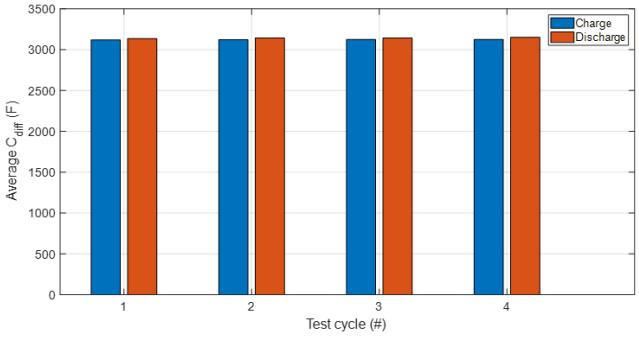


**FIGURE 8.** Evolution of the differential capacitance averaged over the measured voltage range (see Figure 7) of the Maxwell cell during the four CD cycles at ±120 A. The $C_{\text{diff}}$ values estimated during each charge and discharge phase are separately reported.

## IV. CIRCUIT MODELS OF SC CELLS

A reliable cell model is essential for the design and the optimization of practical SC systems employing multiple cells. For proper exploitation, the model should be built in the form of an equivalent circuit. A compromise needs to be found

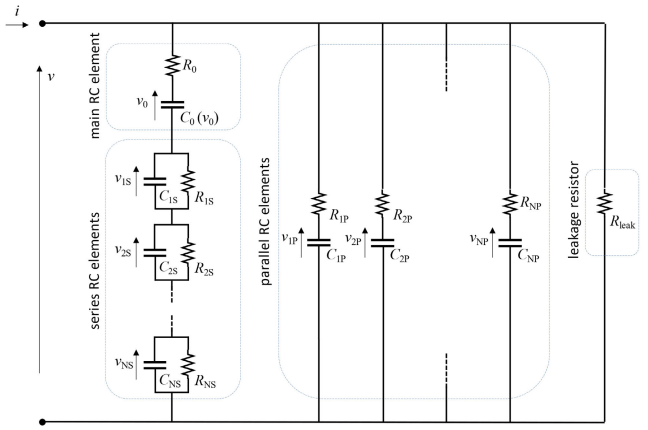


**FIGURE 9.** General equivalent circuit of a SC cell assumed in this paper.

between the accuracy, the simplicity and the robustness of the parameters' identification procedure. The equivalent circuit model of the commercial cells is discussed in this section. An empirical model able to reproduce the measured behavior in the whole test current range is looked for and the parameters of the model are listed for practical use.

A wide variety of phenomenological circuit models of the SC cells is published in the literature [16]–[32]. Several studies exist that analyze and compare the performance of the different models [2], [19], [28]. The vast majority of the different models proposed in the literature can be grouped in the equivalent high-order circuit shown in Figure 9. The different components of the equivalent circuit of Figure 9 (highlighted with boxes) are described in detail in the following subsections. The relation between this equivalent circuit and the different equivalent circuits reported in the literature is discussed in detail at the end of this section.

### A. MAIN RC ELEMENT

A series resistive-capacitive element, denoted with $R_0C_0$ in Figure 9. The main RC element captures the main phenomenology of the cell, that is the observed capacitive behavior and sharp voltage drop corresponding to the switch of the current. As discussed in Section III.E, the capacitor $C_0$ is nonlinear as its capacitance depends on the voltage $v_0$ across it. A linear dependence of the main capacitance $C_0$ on the voltage $v_0$ is usually assumed in SC models [2], [24], [25], which gives

$$C_0(v_0) = C_0(V_r) + k_v(v_0 - V_r) \tag{9}$$

where $V_r$ is the rated voltage of the cell (2.7 V, see Table 1) and $C_0(V_r)$ is the corresponding capacitance [18]. While this main RC branch accounts for the gross behavior of the cell, refined results can be obtained by including further branches in the equivalent circuit, as described in the following.

### B. SERIES RC ELEMENTS

A number $N_S$ of RC elements connected in series to the main RC element and denoted with $R_{1s}C_{1s}$, $R_{2s}C_{2s}$, …, $R_{Ns}C_{Ns}$ in Figure 9. These elements account for the fast transients occurring in the cell. In particular, they add fast exponential modes in the natural response of the circuit that are essential for accurately reproducing the fast change of the cell's voltage during the resting intervals following the step change of the current (see the insert of Figure 2). The series RC elements also account for the frequency dependence of the equivalent resistance, and in particular for the reduced value of the AC resistance with respect to the DC one [2], [29]–[32].

In principle, a high number $N_S$ of RC pairs need to be added, in series to the main RC element, in order to reproduce the transients occurring in the cell on a very short time scale (or, equivalently, over a wide frequency range). However, in practice, a limited $N_S$ allows to reproduce with good accuracy the cell's behavior observed in the experimental tests [32].

### C. PARALLEL RC ELEMENTS

A number $N_P$ of RC elements connected in parallel to the first branch of the equivalent circuit and denoted with $R_{1p}C_{1p}$, $R_{2p}C_{2p}$, …, $R_{Np}C_{Np}$ in Figure 9. These elements account for the slow transients and the non-ideal coulombic behavior of the cell, while have a negligible impact on the high frequency behavior. In practice a few parallel RC pairs, along with the main RC element, allows reproducing with good accuracy the observed cell's behavior during slow changing conditions (for example, constant current operation).

It is worth to report that if only the main and the series RC elements are considered in the equivalent circuit, the voltage of the cell would not be cyclic in case of non-ideal coulombic efficiency. In fact, the latter implies a net charge transfer from the negative to the positive pole at the end of the cycle that would result into an increase of the cell's voltage at the end of the cycle. By adding the parallel branches, charge redistribution can occur, with slow time constants, among the capacitors and the situation that is experimentally observed (recovery of the initial voltage despite the net charge supplied to the cell in one cycle) can be reproduced. Due to this charge redistribution, the parallel RC elements also has a substantial impact on the short-term self-discharge behavior of the cell, occurring on the time scale of the minutes.

### D. LEAKAGE RESISTOR

The paralleled resistor $R_{leak}$ is finally added in the equivalent circuit in order to account for the self-discharge behavior of the cell, occurring on a typical time scale of weeks. This resistor has a strong impact on the slowest exponential mode of the natural response of the circuit, whereas it has negligible impact on all the faster time constants. This means that the value of the leakage resistor only affects the long-term self-discharge characteristic of the cell without impacting the dynamic behavior.

As already stated, the general equivalent circuit model of Figure 9 is obtained by combining the different models proposed in the literature. More in particular, the classical Zubieta and Bonert model [23] and the "parallel model" presented in [27] consist of the parallel RC elements of the equivalent circuit of Figure 10. Similarly, the "dynamic model"

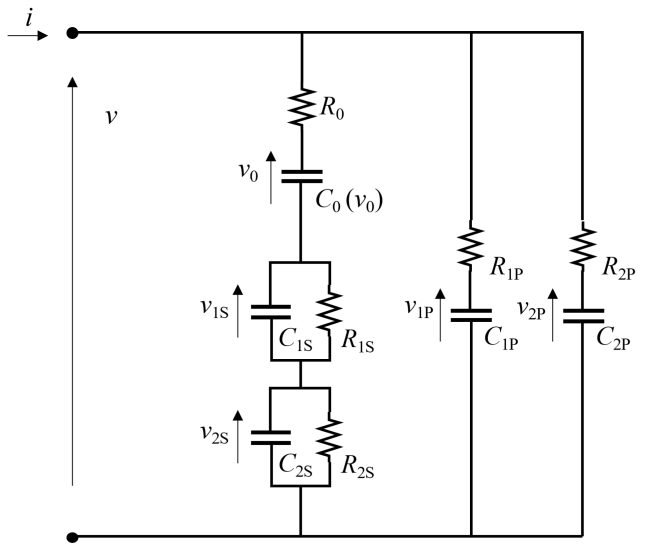


**FIGURE 10.** Adopted equivalent circuit of the large commercial cells to be fitted by the data of the experimental tests.

proposed in [2], [11], [28], the ''series model'' proposed in [2], [4], [20], [29], [30] and the ''Thevenin model'' proposed in [20], [31] consist of the series RC element included in the equivalent circuit of Figure 9. In the series model proposed in [29] and in [4], [32], the capacitances $C_{1s}$, $C_{2s}$, ..., $C_{Ns}$ and the resistances $R_{1s}$, $R_{2s}$, ..., $R_{Ns}$ of the series elements are related to the capacitance $C_0$ of the main RC element via the series expansion of the impedance model of the porous electrodes. In [32] series and parallel elements are combined obtaining a complete equivalent circuit of the type of the one in Figure 9.

The general equivalent circuit of the SC shown in Figure 9 can be made arbitrarily complex by adding more series and parallel RC elements. However, as it is discussed in detail in the next section, a limited number of elements is able to reproduce with appropriate accuracy the behavior of the cell in the whole operating regime investigated in this paper.

## V. EQUIVALENT CIRCUIT AND PARAMETERS OF THE COMMERCIAL SC CELLS

Moving from the general circuit in Figure 9, the equivalent circuit shown in Figure 10 was developed for the commercial SC cells. This is a fifth order circuit consisting of the main RC branch, two series RC elements and two parallel RC elements. As discussed in the following, this equivalent circuit was obtained by gradually increasing the circuit's order and complexity and allowed to achieve a good compromise between the fitting of the measured data and the model simplicity. We have in fact observed that adding more elements in parallel or in series increases the complexity of the equivalent circuit without producing appreciable improvement of the results accuracy. The leakage resistance is not included in the circuit since this only affects the very long term (weeks) behavior of the cell, which is out of the scope of the paper and of the test procedure.

### A. IDENTIFICATION PROCEDURE

The complete definition of the equivalent circuit in Figure 10 requires the identification of 11 parameters, that are:

- The main capacitance $C_0$ at $V_r$ (or equivalently any other voltage value);
- The slope $k_v$ of the voltage-dependent capacitance $C_0$;
- The main resistance $R_0$;
- The two pairs of capacitances $C_{1S}$, $C_{2S}$ and resistances $R_{1S}$, $R_{2S}$ of the series RC elements (4 parameters in total);
- The two pairs of capacitances $C_{1P}$, $C_{2P}$ and resistances $R_{1P}$, $R_{2P}$ of the parallel RC elements (4 parameters in total).

The main parameters of the SC equivalent circuits proposed in the literature are typically identified by specific formulae and measurement procedures [23], [32]. In this paper, the parameters of the proposed model were obtained, for each testing current, by fitting the model generated data onto the experimental data of all the CD cycles by means of the non-linear least square solver *lsqnonlin* in MATLAB [40]. The model data are generated by supplying the equivalent circuit of Figure 10 with the dataset of current measured during the experiments.

Nevertheless, due to the high number of parameters, a gradual approach must be followed for their reliable identification. This approach takes advantage of the different time scale of the effects produced by the model parameters [23], [32]. In particular:

1. The parameters of the main RC element and the parallel RC elements are first found by neglecting the series RC elements. In practice, the voltage profile measured during the whole CD tests at constant current is first fitted by means of the third order circuit obtained by removing the series RC elements ($C_{1S}$, $R_{1S}$, $C_{2S}$, $R_{2S}$) from the circuit of Figure 10. The third order circuit obtained only involves 7 parameters ($C_0$, $k_v$, $R_0$, $C_{1P}$, $R_{1P}$, $C_{2P}$, $R_{2P}$).
2. Once these parameters are fixed, the parameters of the series RC elements can be obtained by refining the fitting of the voltage during the resting intervals (with zero applied current), in which a fast change occurs, by means of the complete fifth order circuit of Figure 10. Only four parameters ($C_{1S}$, $R_{1S}$, $C_{2S}$, $R_{2S}$) need to be identified during this refinement, whereas the others ($C_0$, $k_v$, $R_0$, $C_{1P}$, $R_{1P}$, $C_{2P}$, $R_{2P}$) are fixed as they were obtained with the previous step.

It is important to stress that for assuring good quality of the fitting and robustness of the identification procedure, the number of parameters needs to be gradually increased and a good guess solution must be used each time. For this reason, the order of the circuit is gradually increased and the results

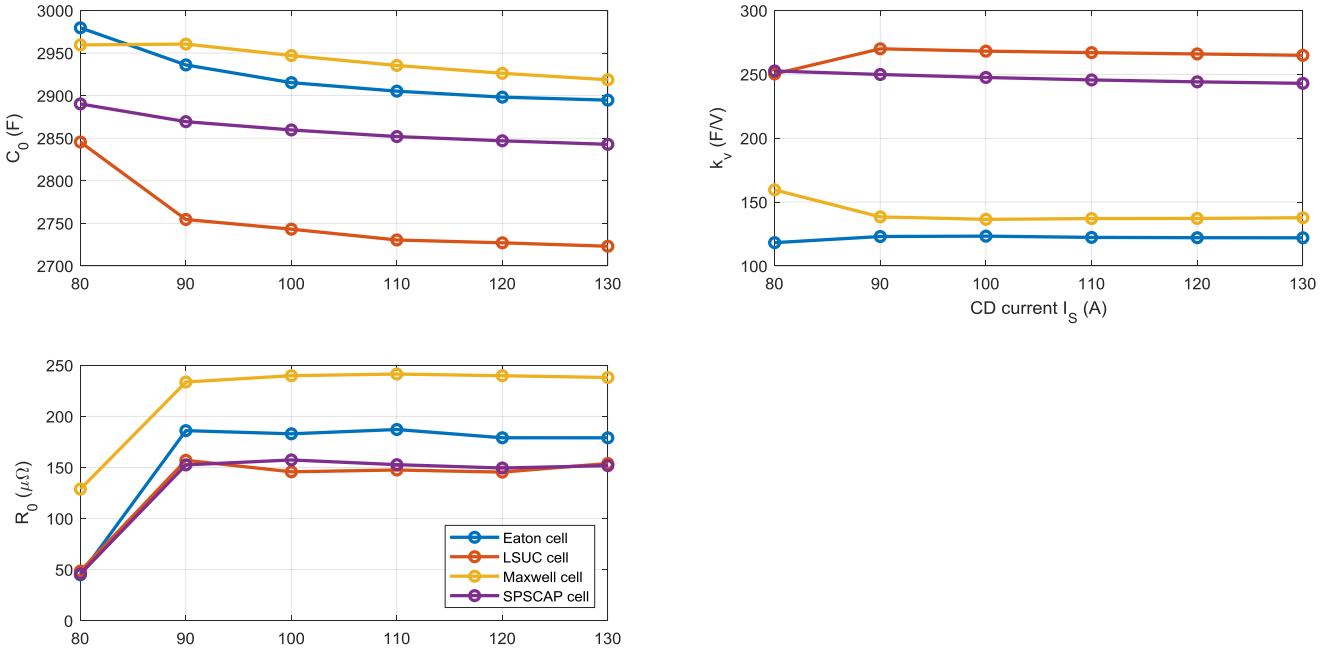


**FIGURE 11.** Parameters $C_0$, $k_V$ and $R_0$ of the equivalent circuit in Figure 10 identified for each of the four commercial SC cells as a function of the cell current. These parameters have similar values for all the cells and are practically independent on the operating current, except the case of the tests performed at ±80 A.

of the solution obtained with the circuit of order $n$ are used as (part of) the initial guess for the circuit with order $n + 1$. In particular, the best fit of the measured data with only the main RC element is first carried out for obtaining a guess solution of parameter $C_0$, $k_v$, $R_0$ at step 1. The first parallel RC element is added and the updated parameters $C_0$, $k_v$, $R_0$, $C_{1P}$, $R_{1P}$ at this new step 2 are calculated using as initial guess the solution at step 1 for $C_0$, $k_v$, $R_0$. The second parallel RC element is then added and the updated parameters $C_0$, $k_v$, $R_0$, $C_{1P}$, $R_{1P}$, $C_{2P}$, $R_{2P}$ at this new step 3 are calculated using as initial guess the solution obtained at step 2 for $C_0$, $k_v$, $R_0$, $C_{1P}$, $R_{1P}$. A similar procedure was used for obtaining the parameters of the series elements. The effect of increasing the circuit order on the accuracy of the results is discussed in Section V.C.

### B. RESULTS OF PARAMETERS IDENTIFICATION

The parameters of the equivalent circuit of the commercial SC cells, obtained by applying the described fitting procedure for all the cells and all the different operating currents, are shown in Figure 11, Figure 12 and Figure 13. These results show that, despite having different model parameters, all the cells follow a similar behavior. Moreover, per each cell, the equivalent circuit is weakly affected by the operating current, except the case of the tests performed at ±80 A. Therefore, the same equivalent circuit with the same parameters can be used for modelling the behavior of a cell in the current range 90-130 A. The average value of the parameters of the equivalent circuit in the range 90-130 A is reported in Table 2 and can be employed to model the cells.

**TABLE 2.** Average value of the parameters of the equivalent circuit of the SC cells obtained with test current in the range 90-130 A.

| Manufacturer | EATON | LSUC | MAXWELL | SPSCAP |
|---|---|---|---|---|
| $C_0$ at 2.7 V (F) | 2744 | 2375 | 2752 | 2522 |
| $k_v$ (F/V) | 123 | 267 | 137 | 246 |
| $R_0$ (mΩ) | 0.183 | 0.150 | 0.239 | 0.153 |
| $C_{1S}$ (F) | 4024 | 2528 | 29763 | 20044 |
| $R_{1S}$ (μΩ) | 39.42 | 21.00 | 24.73 | 45.37 |
| $C_{2S}$ (F) | 511 | 736 | 1136 | 811 |
| $R_{2S}$ (μΩ) | 31.66 | 52.80 | 51.69 | 68.19 |
| $C1_P$ (F) | 117 | 119 | 113 | 90 |
| $R_{1P}$ (Ω) | 0.300 | 0.383 | 0.367 | 0.347 |
| $C_{2P}$ (F) | 2880 | 8167 | 4152 | 1875 |
| $R2_P$ (Ω) | 1.20 | 1.31 | 1.08 | 1.29 |

We report that the identification of the parameters of the main RC element ($C_0$, $k_v$, $R_0$) was very robust for all cells (the same results were obtained independently of the initial guess). This is due to the fact that these parameters have a major impact on the numerical results. A robust identification also occurred for the parameters of the first ($C_{1S}$, $R_{1S}$) and the second ($C_{2S}$, $R_{2S}$) series RC elements, as they affect the change of the voltage after the current switch on a time scale of tens and hundreds of milliseconds, respectively. Similarly, good reproducibility was also obtained for parameters ($C_{1P}$, $R_{1P}$) of the first parallel RC element, as they affect the results on typical time scale of tens of seconds. On the other hand, a greater uncertainty existed for the parameters ($C_{2P}$, $R_{2P}$) of the second parallel RC branch as they affect the free

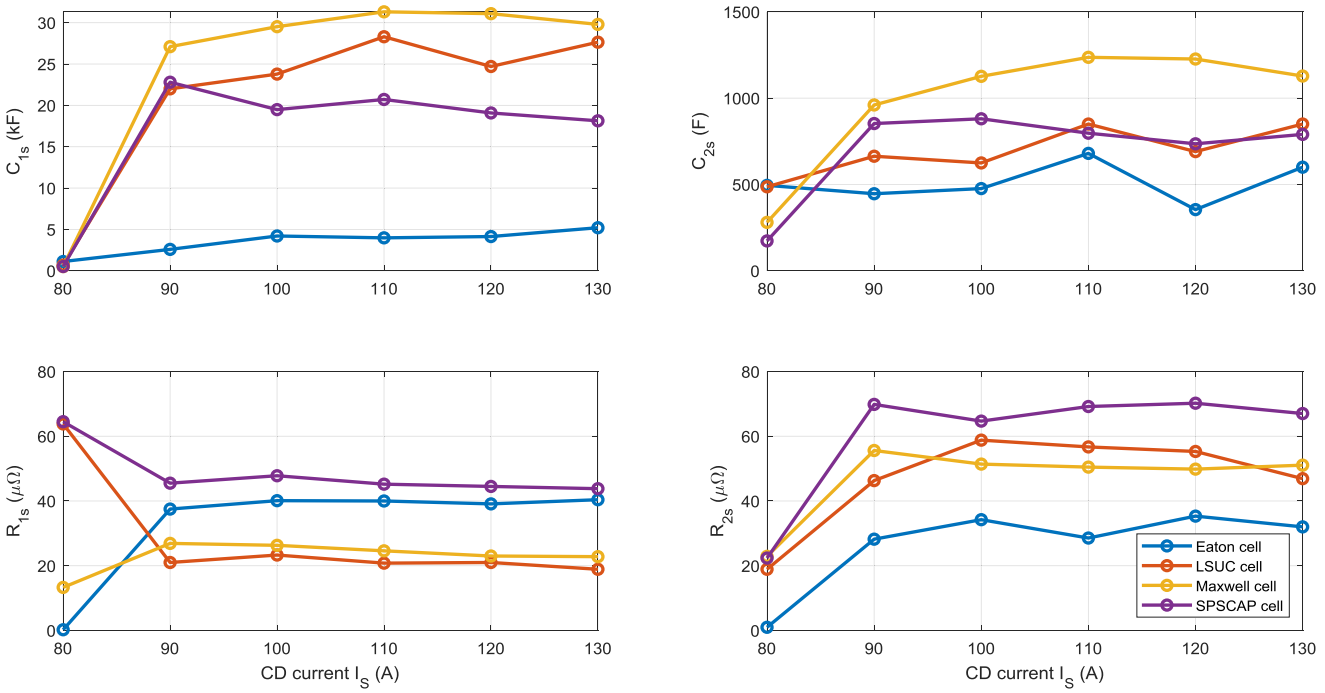


**FIGURE 12.** Parameters $C_{1s}$, $R_{1s}$ and $C_{2s}$, $R_{2s}$ (series elements) of the equivalent circuit in Figure 10 identified for each of the four commercial SC cells as a function of the test current. These parameters have similar values for all the cells and are weakly dependent on the operating current, except the case of the tests performed at ±80 A.

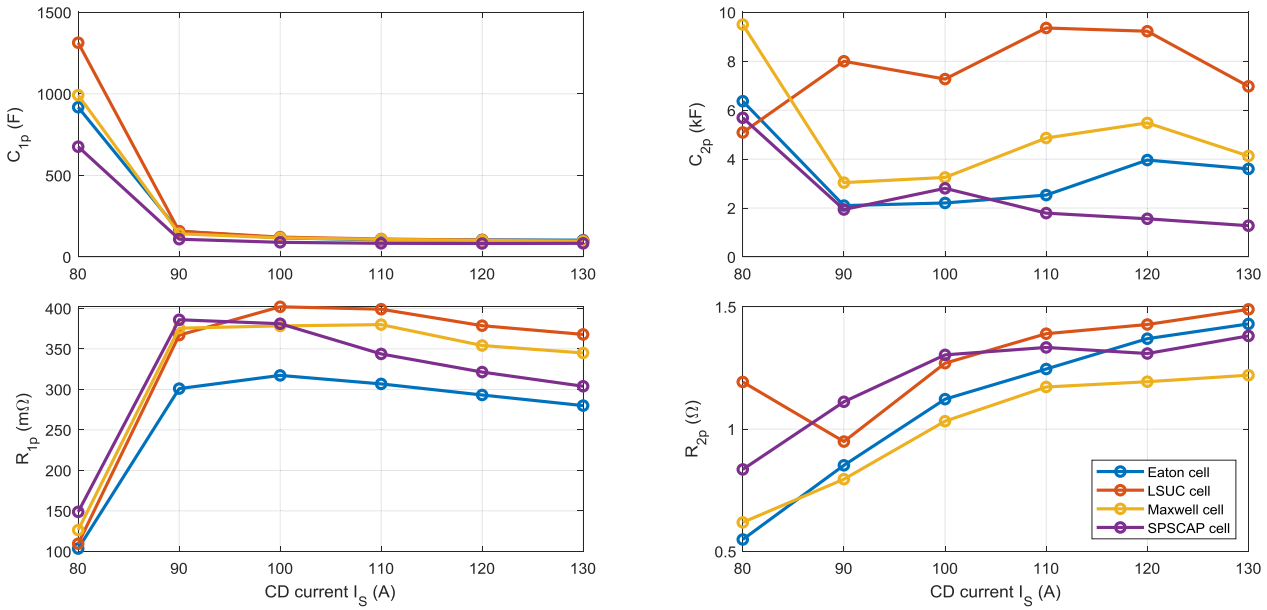


**FIGURE 13.** Parameters $C_{1p}$, $R_{1p}$ and $C_{2p}$, $R_{2p}$ (parallel elements) of the equivalent circuit in Figure 10 identified for each of the four commercial SC cells as a function of the cell current. These parameters have similar values for all the cells. Parameters $C_{1p}$, $R_{1p}$ and $C_{2p}$, are weakly dependent on the operating current, except the case of the tests performed at ±80 A, whereas a more appreciable dependance on the operating current exist for $R_{2p}$.

response of the SC over a time scale of several hundreds of seconds which is much longer than the waiting time of the experiments.

### C. VALIDATION AND DISCUSSION OF MODELING RESULTS

In order to validate the circuit model and the identification approach, the waveforms produced by the numerical simulation of the obtained circuits were compared with the experimental data. As an example, Figure 14 compares the simulated and measured voltages of the Maxwell cell during a CD cycle at ±120 A.

A very good agreement of the modelling and the measured results can be observed, both during the CD phase at constant current and during the transient occurring in the rest intervals

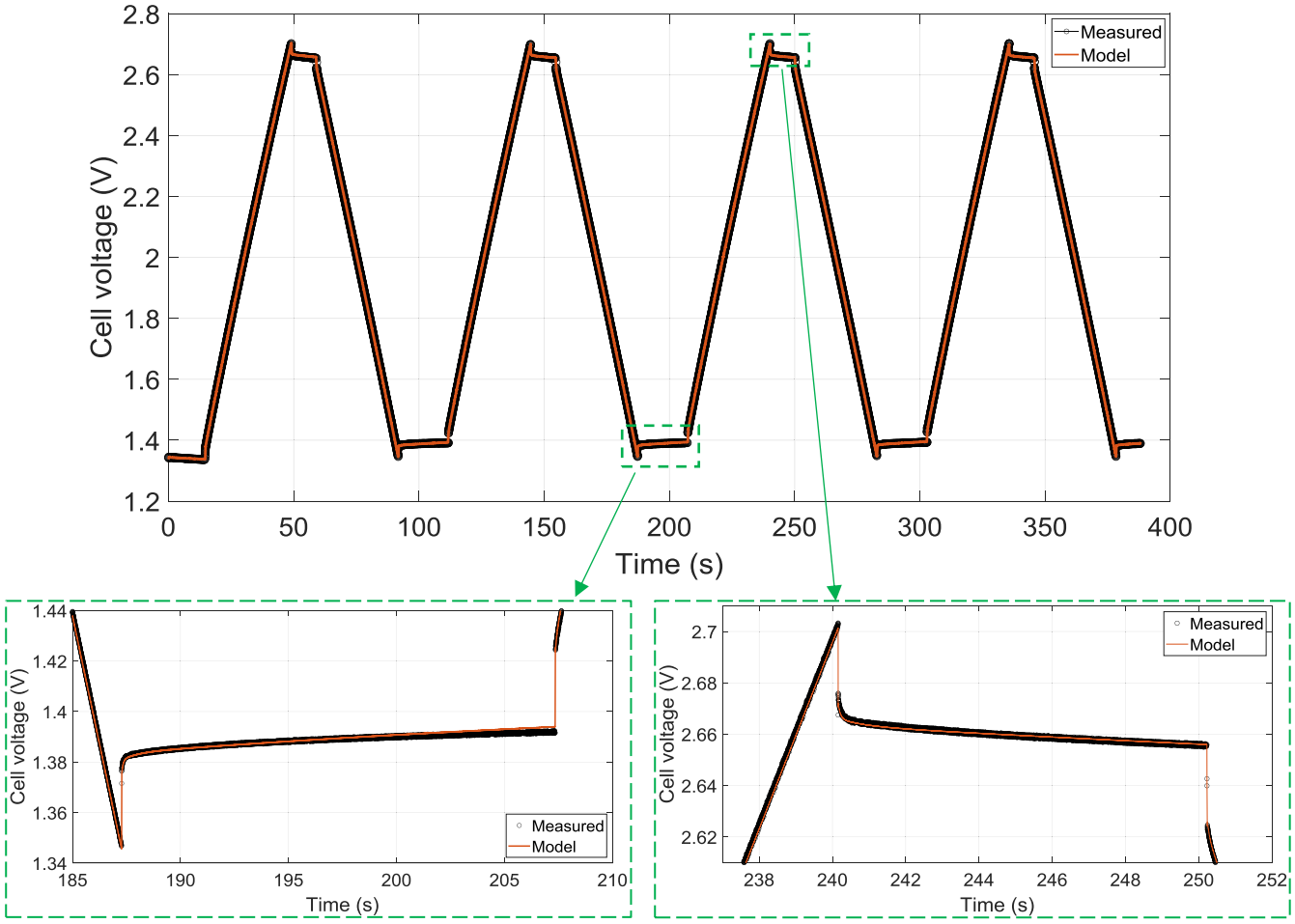


**FIGURE 14.** Comparison between the voltage measured on the Maxwell cell during the four CD cycles at ±120 A and the numerical values obtained by simulations of the developed model.

where no current is applied to the cell (see the inserts of the figure). The very good agreement of the Maxwell cell that can be observed in Figure 14 was found for all the tested currents with the exception of the cases with $I_S = \pm 80$ A. In this latter case, a less accurate reproduction of the measurements was obtained, particularly during the voltage transient occurring in the resting intervals with zero applied current. A similar trend (a very good agreement for all the operating current with the exception of ±80 A) was obtained for all the other cells.

In order to assess the overall quality of the fitting the coefficient of determination $r^2$ is introduced as a global error indicator. It is defined as

$$r^2 = 1 - \frac{\sum_k \left(V_k^{\text{model}} - V_k^{\text{measured}}\right)^2}{\sum_k \left(V_k^{\text{model}} - \bar{V}^{\text{measured}}\right)^2} \tag{10}$$

where $V_k^{\text{model}}$ is the series of the model generated voltages (with $k$ ranging from 1 to the number of measured data points), $V_k^{\text{measured}}$ is the series of the measured voltages, $\bar{V}^{\text{measured}}$ is the average of the measured voltages and the sums extend the whole series of data. The $r^2$ indicator is 1 for a perfect fitting and is 0 if the model generated data are constant and equal to the average. The values of $r^2$ obtained for all cells and all operating currents are shown in Figure 16. It can be seen that an excellent quality of the fitting ($r^2 \sim 1$) is obtained for all cells at high test current (≥90 A). Such an excellent fitting is confirmed also in Figure 15 for the Maxwell cell at ±120 A as an example. However, the quality of the fitting gets worse at ±80 A is considered, meaning that some refinements of the equivalent circuit are required at lower current. It is also worth to notice, in Figure 16, that the quality of the fitting achieved for the LSUC cell is lower than for the other cells.

As already discussed in Section V.A, the equivalent circuit of Figure 10 was obtained by starting from the simple first-order circuit made of the main RC branch and by gradually increasing the circuit's order adding more parallel and series elements. Two parallel elements were first gradually added, thus obtaining a second and a third order circuit, respectively. Two series elements were gradually added, thus obtaining a fourth order circuit and finally the fifth order circuit of Figure 10. Figure 15 compares the data measured for the

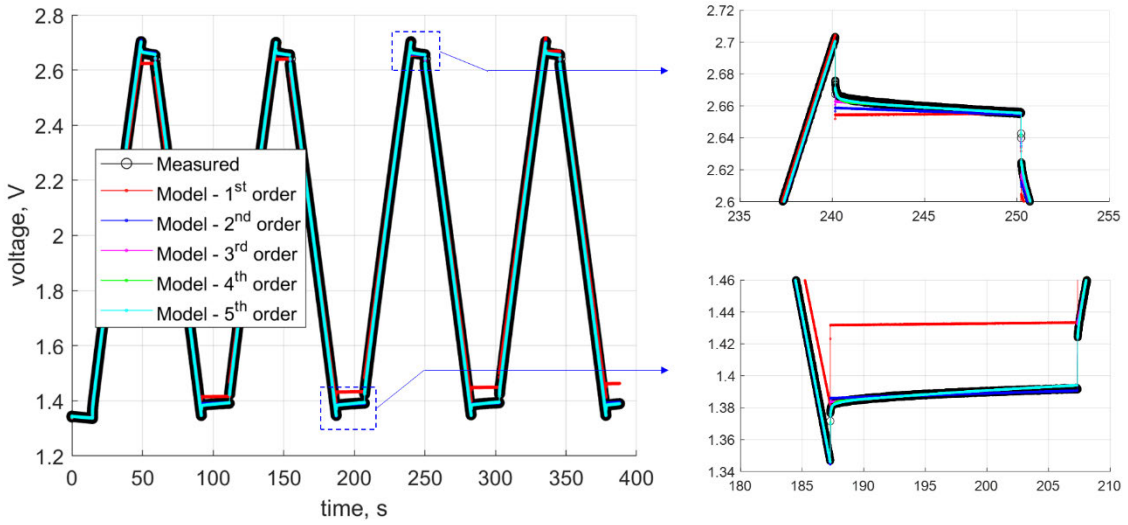


**FIGURE 15.** Numerical results obtained with equivalent circuits of increasing order for the Maxwell cell during four CD cycles at ±120 A. The measured data are also shown for comparison.

Maxwell cell at ±120 with the numerical results obtained for an increasing order of the circuit. At a glance, all the models show a good overall capability to reproduce the cell's behavior, with the exception of the first-order circuit, consisting of the main RC element only, whose results gradually depart form the measured data. However, by the more careful analysis shown in the insert of the figure, it can be observed that a higher accuracy concerning the voltage drop at the switch of the current is obtained by adding more parallel elements. Nevertheless, despite of the better accuracy, a step change of the voltage is obtained at this switch if parallel elements only are added. The fast transient behavior, corresponding to the exponential decay of the voltage, can be reproduced, with increasing accuracy, only if the series elements are added. Series elements are then essentials if good prediction of the cell at high frequency regimes is required [32].

### D. EQUIVALENT RESISTANCES OF THE COMMERCIAL CELLS

The SC datasheets always report one single equivalent resistance $R_{\mathrm{ESR}}$ (see Table 1), whereas circuit models include several resistors.

In practice, the total resistance of the first branch of the equivalent circuit, involving resistors $R_0$ and $R_{1\mathrm{s}}$, …, $R_{N\mathrm{s}}$, provides the main contribution to the $R_{\mathrm{ESR}}$ and can be regarded as the resistance $R_{\mathrm{DC}}$ of the cell at low frequency, corresponding to the sum of the resistances of the main and the series branches [4], [32]. For the equivalent circuit in Figure 10 the resistance $R_{\mathrm{DC}}$ is given by

$$R_{\mathrm{DC}} \cong R_0 + R_{1s} + R_{2s} \tag{11}$$

The values of $R_{\mathrm{DC}}$ obtained for each cell and each testing current are shown in Figure 17. These values are consistent

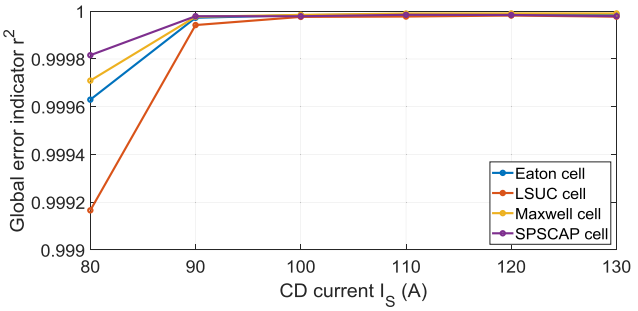


**FIGURE 16.** Global error indicator of the fitted data of the equivalent circuit for all cells at the different currents.

with the ESR values declared in the manufacturers' datasheet (also reported in Figure 17 and Table 1). The difference among the $R_{\mathrm{DC}}$ values and the specified ESRs is presumably due the different followed test procedures. In fact, according to the IEC 62391-1 [15] the test current should be $0.4{\cdot}C_{\mathrm{r}}{\cdot}V_{\mathrm{r}} \approx 3$ A or $4{\cdot}C_{\mathrm{r}} \cdot V_{\mathrm{r}} \approx 32$ A for a continuous energy storage or power application, respectively, that are both much lower than the test currents used in this paper. The resistance data in Figure 17 are also consistent with the cell performances in terms of efficiency, as the main part of the dissipation occurs in the first branch of the equivalent circuit. In particular, the slightly higher value of $R_{\mathrm{DC}}$ found for the Maxwell cell is consistent with the slightly lower efficiency found in Figure 5.

However, the lower resistance in Figure 17 for the test current of 80 A for all cells is in conflict with the lower efficiency reported in Figure 5. At this regard, it is worth to point out that, as discussed in Section VI.B, the quality of the fitting and, hence, the accuracy of the numerical results at 80 A is not as good as for the other cases. Then, the equivalent

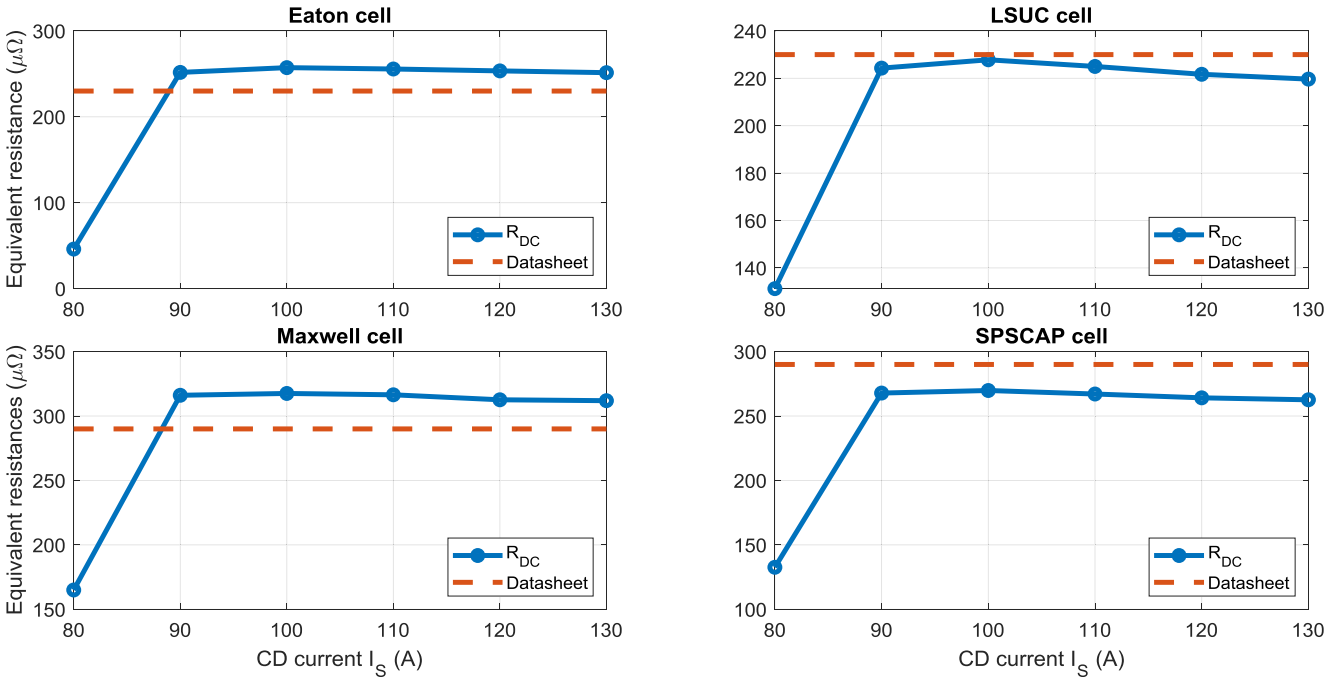


**FIGURE 17.** Comparison between the equivalent resistances estimated for the four commercial SC cells as a function of the cell current and the equivalent resistance reported in the manufacturer datasheets.

circuit of Figure 10 with the parameters of Table 2 should be used for quantitative evaluations only in the range 90-130 A, where the accuracy is excellent.

## VI. CONCLUSION

Most of the characterization and modelling studies reported in the literature apply test currents that are very limited with respect to practical operating current of SC cells. As the current affects the behavior of the cell, it is important to characterize the cell at realistic current level and to develop and validate the model accordingly. In this paper, CD test cycles of large commercial SC cells (3000 F) were performed with current level in the range 80-130 A, which is close the maximum rated current of the cells. The test results were used to assesses and compare the performance of the SC cells in terms of energy efficiency, coulombic efficiency and differential capacitance. An equivalent circuit of the cells, able to reproduce the experimental behavior in the whole tested current range, was also developed. The parameters of the model were identified by means of the fitting of the measured data. All the investigated commercial cells were found to comply with the same circuit model, with circuit parameters in the same range and weakly dependent on the test current. The accuracy of the numerical results was found to be excellent for test currents in the range 90-130 A, whereas a lower accuracy was found for the lower tested current of 80 A. The parameters obtained for all the cells were clearly listed in the paper to make them exploitable in practical applications.

## REFERENCES

[1] J. M. Miller, *Ultracapacitor Applications*. Bangalore, India: Inst of Engineering & Technology, 2011.

[2] A. Berrueta, A. Ursua, I. S. Martin, A. Eftekhari, and P. Sanchis, "Supercapacitors: Electrical characteristics, modeling, applications, and future trends," *IEEE Access*, vol. 7, pp. 50869–50896, 2019, doi: 10.1109/ACCESS.2019.2908558.

[3] A. Lampasi, G. Taddia, S. M. Tenconi, and F. Gherdovich, "Compact power supply with integrated energy storage and recovery capabilities for arbitrary currents up to 2 kA," *IEEE Trans. Plasma Sci.*, vol. 46, no. 10, pp. 3393–3400, Oct. 2018.

[4] F. Castelli Dezza, V. Musolino, L. Piegari, and R. Rizzo, "Hybrid battery–supercapacitor system for full electric forklifts," *IET Electr. Syst. Transp.*, vol. 9, no. 1, pp. 16–23, Mar. 2019, doi: 10.1049/iet-est.2018.5036.

[5] F. Ortenzi, M. Pasquali, P. P. Prosini, A. Lidozzi, and M. Di Benedetto, "Design and validation of ultra-fast charging infrastructures based on supercapacitors for urban public transportation applications," *Energies*, vol. 12, p. 2348, Jan. 2019.

[6] D. P. Dubal, O. Ayyad, V. Ruiz, and P. Gomez-Romero, "Hybrid energy storage: The merging of battery and supercapacitor chemistries," *Chem. Soc. Rev.*, vol. 44, no. 7, pp. 1777–1790, 2015.

[7] D. Shin, Y. Kim, J. Seo, N. Chang, Y. Wang, and M. Pedram, "Battery-supercapacitor hybrid system for high-rate pulsed load applications," in *Proc. Design, Autom. Test Eur., Grenoble*, 2011, pp. 1–4, doi: 10.1109/DATE.2011.5763295.

[8] Y. S. Perdana, S. M. Muyeen, A. Al-Durra, H. K. Morales-Paredes, and M. G. Simoes, "Direct connection of supercapacitor–battery hybrid storage system to the grid-tied photovoltaic system," *IEEE Trans. Sustain. Energy*, vol. 10, no. 3, pp. 1370–1379, Jul. 2019, doi: 10.1109/TSTE.2018.2868073.

[9] A. Lahyani, P. Venet, A. Guermazi, and A. Troudi, "Battery/supercapacitors combination in uninterruptible power supply (UPS)," *IEEE Trans. Power Electron.*, vol. 28, no. 4, pp. 1509–1522, Apr. 2013, doi: 10.1109/TPEL.2012.2210736.

[10] P. Kurzweil, M. Chwistek, and R. Gallay, "Electrochemical and spectroscopic studies on rated capacitance and aging mechanism of supercapacitors," in *Proc. 2nd Eur. Symp. Super CapacitorS Appl. (ESSCAP)*, Lausanne, Switzerland, Nov. 2006, pp. 2–3.

[11] N. Devillers, S. Jemei, M. Pera, D. Bienaime, and F. Gustin, "Review of characterization methods for supercapacitor modelling," *J. Power Sources*, vol. 246, pp. 596–608, Jan. 2014, doi: 10.1016/j.jpowsour.2013.07.116.

[12] Y. Wang, Y. Song, and Y. Xia, "Electrochemical capacitors: Mechanism, materials, systems, characterization and applications," *Chem. Soc. Rev.*, vol. 45, no. 21, pp. 5925–5950, 2016.

[13] A. Laheaar, P. Przygocki, Q. Abbas, and F. Beguin, "Appropriate methods for evaluating the efficiency and capacitive behavior of different types of supercapacitors," *Electrochem. Commun.*, vol. 60, pp. 21–25, Nov. 2015, doi: 10.1016/j.elecom.2015.07.022.

[14] F. Rafik, H. Gualous, R. Gallay, A. Crausaz, and A. Berthon, "Frequency, thermal and voltage supercapacitor characterization and modeling," *J. Power Sources*, vol. 165, no. 2, pp. 928–934, 2007, doi: 10.1016/j.jpowsour.2006.12.021.

[15] *Fixed Electric Double-Layer Capacitors for Use in Electric and Electronic Equipment—Part 1: Generic Specification*, document IEC-62391-1, 2015.

[16] Y. Zhao, W. Xie, Z. Fang, and S. Liu, "A parameters identification method of the equivalent circuit model of the supercapacitor cell module based on segmentation optimization," *IEEE Access*, vol. 8, pp. 92895–92906, 2020, doi: 10.1109/ACCESS.2020.2993285.

[17] D. Xu, L. Zhang, B. Wang, and G. Ma, "Modeling of supercapacitor behavior with an improved two-branch equivalent circuit," *IEEE Access*, vol. 7, pp. 26379–26390, 2019, doi: 10.1109/ACCESS.2019.2901377.

[18] A. Cocchi and A. Lampasi, "Modeling non-ideal behaviors of Supercapacitors' equivalent capacitance," in *Proc. IEEE Int. Conf. Environ. Electr. Eng.*, Madrid, Spain, Jun. 2020, pp. 9–12.

[19] L. Zhang, X. Hu, Z. Wang, F. Sun, and D. G. Dorrell, "A review of supercapacitor modeling, estimation, and applications: A control/management perspective," *Renew. Sustain. Energy Rev.*, vol. 81, no. 2, pp. 1868–1878, 2018, doi: 10.1016/j.rser.2017.05.283.

[20] H. Miniguano, A. Barrado, C. Fernandez, P. Zumel, and A. Lazaro, "A general parameter identification procedure used for the comparative study of supercapacitors models," *Energies*, vol. 12, p. 1776, May 2019.

[21] F. Gherdovich, G. Taddia, S. Tenconi, M. Pretelli, A. Lampasi, F. Soavi, F. Poli, A. Morandi, P. L. Ribani, C. Rossi, U. Melaccio, and M. L. Di Vona, "Test and modeling of commercial supercapacitors for pulsed power supplies," in *Proc. 4th Int. Workshop Supercapacitors Energy Storage*, Bologna, Italy, Jun. 2019, pp. 27–28.

[22] F. Gherdovich, G. Taddia, S. Tenconi, M. Pretelli, A. Lampasi, F. Soavi, and M. L. Di Vona, "Comparison and modeling of commercial supercapacitors via standardized potentiostatic electrochemical impedance spectroscopy," in *Electrimacs* (Lecture Notes in Electrical Engineering), vol. 604, W. Zamboni and G. Petrone, Eds. Cham, Switzerland: Springer, 2020, pp. 681–683.

[23] L. Zubieta and R. Bonert, "Characterization of double-layer capacitors for power electronics applications," *IEEE Trans. Ind. Appl.*, vol. 36, no. 1, pp. 199–205, 2000, doi: 10.1109/28.821816.

[24] C. T. Goh and A. Cruden, "Bivariate quadratic method in quantifying the differential capacitance and energy capacity of supercapacitors under high current operation," *J. Power Sources*, vol. 265, pp. 291–298, Dec. 2014, doi: 10.1016/j.jpowsour.2014.04.139.

[25] Y. Diab, P. Venet, H. Gualous, and G. Rojat, "Electrical, frequency and thermal mea-surement and modelling of supercapacitor performance," in *Proc. ESSCAP*, Rome, Italy, Nov. 2008, pp. 1–9.

[26] Y. Parvini, J. B. Siegel, A. G. Stefanopoulou, and A. Vahidi, "Supercapacitor electrical and thermal modeling, identification, and validation for a wide range of temperature and power applications," *IEEE Trans. Ind. Electron.*, vol. 63, no. 3, pp. 1574–1585, Mar. 2016, doi: 10.1109/TIE.2015.2494868.

[27] C. Quintans, R. Iglesias, A. Lago, J. M. Acevedo, and C. Martinez-Penalver, "Methodology to obtain the voltage-dependent parameters of a fourth-order supercapacitor model with the transient response to current pulses," *IEEE Trans. Power Electron.*, vol. 32, no. 5, pp. 3868–3878, May 2017, doi: 10.1109/TPEL.2016.2593102.

[28] L. Zhang, X. Hu, Z. Wang, F. Sun, and D. G. Dorrell, "A comparative study of equivalent circuit models of ultracapacitors for electric vehicles," *J. Power Sources*, vol. 274, pp. 899–906, Jun. 2015, doi: 10.1016/j.jpowsour.2014.10.170.

[29] S. Buller, E. Karden, D. Kok, and R. W. De Doncker, "Modeling the dynamic behavior of supercapacitors using impedance spectroscopy," in *Proc. Conf. Rec. IEEE Ind. Appl. Conf.*, Chicago, IL, USA, Dec. 2002, pp. 2500–2504, doi: 10.1109/IAS.2001.955972.

[30] C. H. Wu, Y. H. Hung, and C. W. Hong, "On-line supercapacitor dynamic models for energy conversion and management," *Energy Convers. Manage.*, vol. 53, no. 1, pp. 337–345, 2012, doi: 10.1016/j.enconman.2011.01.018.

[31] M. Michalczuk, L. M. Grzesiak, and B. Ufnalski, "Experimental parameter identification of battery-ultracapacitor energy storage system," in *Proc. IEEE 24th Int. Symp. Ind. Electron. (ISIE)*, Buzios, Brazil, Jun. 2015, pp. 1260–1265, doi: 10.1109/ISIE.2015.7281653.

[32] V. Musolino, L. Piegari, and E. Tironi, "New Full-Frequency-Range supercapacitor model with easy identification procedure," *IEEE Trans. Ind. Electron.*, vol. 60, no. 1, pp. 112–120, Jan. 2013, doi: 10.1109/TIE.2012.2187412.

[33] (Nov. 2017). *EATON—Supercapacitors Cylindrical cell, Technical Data 10339*. [Online]. Available: https://www.eaton.com/content/dam/eaton/products/electronic-components/resources/data-sheet/eaton-xl60-supercapacitors-cylindrical-cells-data-sheet.pdf

[34] (2017). *LS ULTRACAPCITOR (LSUC)—Product Specification*. [Online]. Available: https://www.ultracapacitor.co.kr:8001/sub/product/LSUC/LSUC002R7C_cylindrical.pdf

[35] *MAXWELL—Data Sheet K2 Ultracapacitors—2.7V series*. Accessed: Dec. 18, 2020. [Online]. Available: https://www.maxwell.com/images/documents/k2series_ds_10153704.pdf

[36] *SUPERCAP, SCP STA Data Sheet, 2017, Version: V2017-2*. Accessed: Dec. 18, 2020. [Online]. Available: https://www.spscap.com/Data-Sheet/Data-Sheet_SCP-STA-Series_2017-2_EN-.pdf

[37] *Skeleton Technologies—SKELCAP Ultracapacitors*. Accessed: Dec. 18, 2020. [Online]. Available: https://www.skeletontech.com/skelcap-sca-ultracapacitor-cells

[38] *CapTop—Datasheet 3.0V Cell WL Series*. Accessed: Dec. 18, 2020. [Online]. Available: https://captop.it/wp-content/uploads/2020/11/Datasheet-3.0V-Cell-WL-Series-.pdf

[39] A. Morandi, A. Fiorillo, S. Pullano, and P. L. Ribani, "Development of a small cryogen-free MgB2Test coil for SMES application," *IEEE Trans. Appl. Supercond.*, vol. 27, no. 4, pp. 1–4, Jun. 2017, doi: 10.1109/TASC.2017.2653202.

[40] MathWorks Help Center. *Lsqnonlin—Solve Nonlinear Least-Squares (Nonlinear Data-Fitting) Problems*. Accessed: Dec. 18, 2020. [Online]. Available: https://it.mathworks.com/help/optim/ug/lsqnonlin.html

**ANTONIO MORANDI** (Senior Member, IEEE) received the M.S. degree in electrical engineering from the University of Bologna, Italy, in 1999, and the Ph.D. degree in electrical engineering in 2004.

He is currently an Associate Professor with the Department of Electrical, Electronic, and Information Engineering. His research interests include power applications of superconductors and energy storage. He has coordinated research projects funded by Public Agencies based on Competitive calls and by private companies and has contributed to the prototyping of superconducting power apparatus (fault current limiters ad superconducting magnetic energy storage) and the development of modeling and design tools. He is author or coauthor of about 60 technical papers published in international journals and conferences. He is also an Inventor of three patents.

Dr. Morandi is a Board Member of ESAS–European Society for Applied Superconductivity. He is an Associate Editor of IEEE TRANSACTIONS ON APPLIED SUPERCONDUCTIVITY.

**ALESSANDRO LAMPASI** (Member, IEEE) received the M.Sc. degree in electronic engineering and the Ph.D. degree in electrical engineering from the University of Rome Sapienza, Rome, Italy, in 2002 and 2006, respectively. He is currently with the Italian National Agency for New Technologies, Energy and Sustainable Economic Development (ENEA), Frascati, Italy, where he is also an in charge of several international projects concerning nuclear fusion, power systems, and energy storage. From ENEA, he is seconded to the consortium for the construction of the Divertor Tokamak Test (DTT) facility. His current research interests include modeling and measurement techniques in the fields of nuclear fusion, power electronics, energy storage, and applied electromagnetics.

**ALESSANDRO COCCHI** received the B.S. degree in mechanical engineering from the University of Rome Roma Tre, in 2015, and the M.S. degree in energy engineering from the University of Rome Tor Vergata, in 2018. He is currently pursuing the Ph.D. degree in engineering and applied science for energy and industry with the University of Rome Sapienza. His research interests include power electronics and energy storage systems.

**FILIPPO GHERDOVIC** received the M.Sc. degree in energetic engineering from the University of Bologna, Italy, in 2015, and the Ph.D. degree in industrial engineering from the University of Rome Tor Vergata, in 2018. After second level master on fusion energy, he carried out at the University of Rome Tor Vergata, conducting researches on supercapacitors issues, as modeling, technology, and industrial applications at OCEM Energy Technology, Bologna. He currently holds the position of Development Engineer at OCEM Energy Technology.

**UMBERTO MELACCIO** was born in Barletta, Italy, in November 1992. He received the B.S. and M.S. degrees in energy engineering from Alma Mater Studiorum, University of Bologna, in 2014 and 2017, respectively, where he is currently pursuing the Ph.D. degree in electrical engineering. His research interest includes the design of superconducting magnet for power applications were partly developed at the department of applied superconductivity of Changwon, South Korea.

**PIER LUIGI RIBANI** (Member, IEEE) was born in Bologna, Italy, in August 1957. He received the M.S. degree in nuclear engineering from the University of Bologna, in 1982. Since 1987, he has been with the University of Bologna, where he is currently a Professor with the Department of Electrical Engineering. His main research interests include several aspects of magnetohydrodynamic, magnetic systems, and applied superconductivity.

**CLAUDIO ROSSI** received the M.Sc. and Ph.D. degrees from the University of Bologna, in 1997 and 2001, respectively, in electrical engineering. Since 2000, he has been a Research Associate with the Department of Electrical Engineering, University of Bologna, in Electrical Machines, Drives, and Power Electronics. He has been an Associate Professor since 2015. His current research interests include devoted to power electronics, electric drives, and battery management system for full-electric and hybrid-electric vehicles.

**FRANCESCA SOAVI** is currently an Associate Professor in inorganic chemistry with the Department of Chemistry ''Giacomo CIamician'', University of Bologna. Her research is carried out with the Laboratory of Electrochemistry of Materials for Energetics (LEME) and CIRI FRAME. She is also the Chair of the Division 3- Electrochemical Energy Storage and Conversion, The International Society of Electrochemistry. She is involved in knowledge transfer of research products by the StartUp BETTERY srl that she co-founded in 2018. She has coauthored more than 110 peer-reviewed articles (H-index 35, more than 4000 citations).